Development of X-ray/gamma-ray imaging spectrometers using reach-through APD arrays

2012 JINST 7 C03038

(http://iopscience.iop.org/1748-0221/7/03/C03038)

JINST

PUBLISHED BY IOP PUBLISHING FOR SISSA MEDIALAB

RECEIVED: *October 31, 2011*
REVISED: *February 5, 2012*
ACCEPTED: *February 27, 2012*
PUBLISHED: *March 20, 2012*

THE 9th INTERNATIONAL CONFERENCE ON POSITION SENSITIVE DETECTORS,
12–16 SEPTEMBER 2011,
ABERYSTWYTH, U.K.

Development of X-ray/gamma-ray imaging spectrometers using reach-through APD arrays

T. Nakamori,[a,1] **T. Enomoto,**[b] **T. Toizumi,**[b] **K. Tokoyoda,**[b] **Y. Yatsu,**[b] **N. Kawai,**[b] **J. Kataoka,**[a] **Y. Ishikawa,**[c] **T. Kawai,**[c] **N. Kawabata**[c] **and Y. Matsunaga**[c]

[a] *Research Institute for Science and Engineering, Waseda University, 3-4-1 Ohkubo, Shinjuku, Tokyo, Japan*
[b] *Faculty of Science and Engineering, Tokyo Institute of Technology, 2-12-1 Ohokayama, Meguro, Tokyo, Japan*
[c] *Solid State Division, Hamamatsu Photonics, K. K., 1126-1 Ichino-cho, Hamamatsu, Shizuoka, Japan*

E-mail: nakamori@aoni.waseda.jp

ABSTRACT: We present spectroscopic capability of a position sensitive detector using a large area reach-through avalanche photodiode (APD) array, mainly for astronomical applications. It is quite important to obtain wide band spectra of high energy astrophysical phenomena simultaneously in order to probe emission processes or structures. Especially observations of transient objects, such as gamma-ray bursts of active galactic nuclei, require detectors with wide energy band coverage for the sake of an efficient spectroscopy within limited time windows. An APD is a compact semiconductor photon sensor with an internal gain which is often up to $\sim$100. A reach-through type APD has a thicker depletion layer thus higher efficiency for direct X-ray detection compared to a reverse type APD. We have developed 1-dimensional reach-through APD arrays which consist of 8 and 16 segments with a pixel size of 2.2×16 and 1.1×16 mm^2. We demonstrated quite uniform gain and energy resolution for 5.9 keV X-ray over the pixels of these arrays. Subsequently we constructed X-ray/gamma-ray detector using the APD array optically coupled to a conventional CsI(Tl) scintillator which demonstrated energy coverage typically from 1 keV to 1 MeV.

KEYWORDS: Imaging spectroscopy; X-ray detectors and telescopes; Gamma detectors

[1] Corresponding author.

doi:10.1088/1748-0221/7/03/C03038

Contents

2012 JINST 7 C03038

1 Introduction

Silicon-based semiconductor devices have made huge progress in the recent past and their applications are spread widely among different experimental physics fields such as particle physics, astrophysics and medical physics. Avalanche photo diodes (APDs) are such semiconductor device, having high quantum efficiency of $\sim$80% at $\sim 400-800$ nm and fast response typically < 1 nsec. Moreover, APDs are characterized by an internal signal amplifying function which is realized by a strong gradient of an electric field in a depletion layer. Ikagawa et al.(2003) [1] reported detailed studies of basic characteristics of reverse-type APDs, which are optimized for detection of scintillation light, in applications for X-ray and gamma-ray detectors with inorganic scintillators [2]. Although APDs have a disadvantage of gain variability depending on its temperature, Kataoka et al.(2006) [3] introduced an active gain control under moderate temperature variations. Utilizing advanced gain control system, recently in-orbit operation of an APD is successfully demonstrated by a pico-satellite *Cute 1.7+APD II* [7] as a charged particle counter in low earth orbit. The characteristics of APDs, namely the compactness and low power consumption, are great advantage in space missions, where space and power are strictly constrained. For instance, APDs will be applied, as readout photo sensors for BGO scintillators, to Hard X-ray Imager [5] and Soft Gamma-ray Detector [6] onboard *ASTRO-H* [4], which is the next generation of Japanese X-ray observatory to be launched in 2014.

A reach-through type APD has a thicker depletion layer (> 100 μm), a large part of which works as a photon-absorbing and electron-drifting layer. The rest of the depletion layer as much as 10% in its total volume located at its thin n-side end causes an avalanche amplification of charge carriers with its high electric field strength. Therefore every signal is uniformly amplified when photons are absorbed anywhere in the depletion layer. On the other hand, dark currents are a little higher than reverse-type APDs because the reach-through APD inevitably also multiplies a large number of thermal electrons. Detailed study of reach-through APD is given in Yatsu et al.(2006) [8].

Table 1. Characteristics of the APD array at 25°C.

Number of pixels	8	16
Surface area	$16 \times 19\,\mathrm{mm}^2$	$16 \times 22\,\mathrm{mm}^2$
Width of a pixel	2.2 mm	1.1 mm
Breakdown bias	578 V	348 V
Bias voltage (Gain=20)	464 V	254 V
Dark current (Gain=20)	4 nA/ch	20 nA/ch
Capacitance (Gain=20)	30 pF/ch	19 pF/ch

In the field of X-ray astronomy, coded aperture photometry combined with position-sensitive detectors are performed by several missions, which decides direction of incident photons from 'pattern of shadows' made by randomly patterned mask (coded mask) above the detector. For instance, *High Energy Transient Explorer-2 (HETE-2)* satellite launched in 2000 operated the Wide-Field X-ray Monitor (WXM) [9], which consisted of a one-dimensional coded mask and two 1-D position-sensitive proportional counters (PSPCs). Each PSPC contains Xe gas with CO_2 as quencher and encodes the X- and Y- position of incident photons along with the energy.

Extending this conventional approach, we consider a new detector using reach-through APDs as a position sensitive detector. We have already developed a wideband X-ray/gamma-ray spectrometer with Hamamatsu reach-through APD SPL 5767 covering typically from 1 keV to 1 MeV [10]. The detector is composed of a 5×5 mm^2 APD and a CsI(Tl) scintillator of $6 \times 6 \times 6$ mm^3 which is optically coupled at the p-side of the APD. The n-side of the APD is exposed to incident photons so that lower energy X-rays ($<$ a few 10 keV) are directly detected by the APD. On the other hand higher energy gamma-rays penetrate the APD and are absorbed in the CsI(Tl) crystal when the APD is also used for the detection of the scintillation light. These signals are discriminated by utilizing the difference in a characteristic rise time which is $\sim$1 ns and 2 μs for the APD and CsI(Tl) scintillation, respectively. The signal from the APD is fed into a charge sensitive amplifier and subsequently divided to a fast ($\tau = 50$ ns) and slow ($\tau = 2$ μs) shaping amplifier. See [10] for more detail.

2 APD array

2.1 8 channel array

Figure 1 shows photograph of the reach-through APD 7003 manufactured by Hamamatsu. Characteristic parameters are listed in table 1, measured at 25°C at Hamamatsu. Each APD has segmented 8 and 16 pixels of 2.2 mm and 1.1 mm wide, respectively, and corresponding cathode terminals. In addition, a common anode terminal is equipped.

First we measured dark currents from each pixels at various bias voltages using the source measure unit (Model 237, Keithley). Hereafter every APD pixel is isolated from other pixels and individually read out in order to avoid contamination from other pixels. Figure 2 shows measured dark currents at various bias voltages under different temperatures of 20, 0, -20°C. The data are

2012 JINST 7 C03038

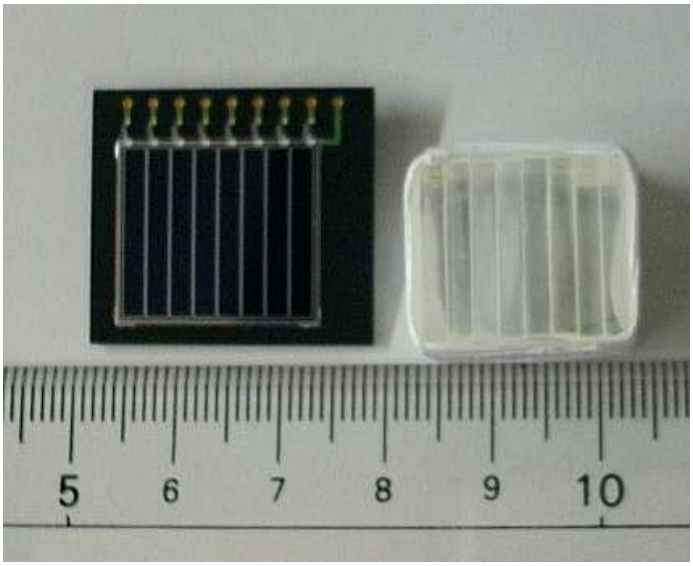

Figure 1. A picture of the 8-channel APD array with a corresponding pixelized CsI(Tl) array. The visible side of the APD is n-side.

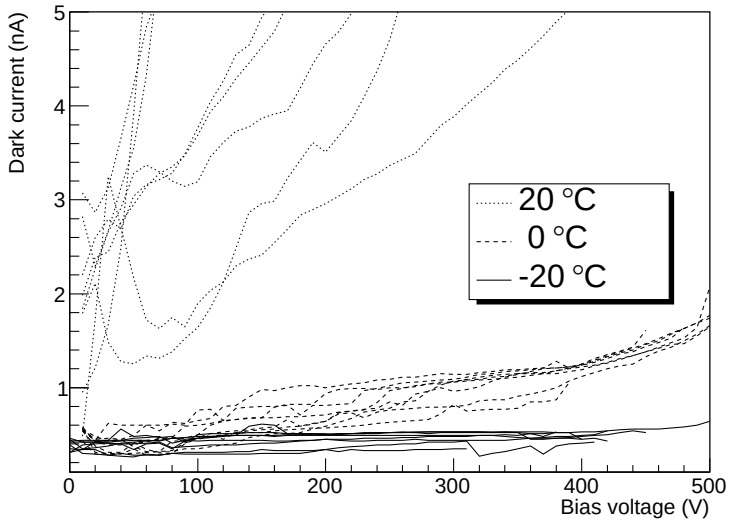

Figure 2. Dark currents for 8 pixels at various bias voltages. Solid, dashed and dotted curves represent measurements at -20, 0, and 20°C, respectively.

taken with 10 V interval, and all the curves are terminated just before the breakdown feature showing rapid increase up to $\gg 1\ \mu$A. All channels show quite uniform and common trend against the bias voltages especially at low temperatures, while some channels go into the breakdown at lower bias voltages than others. This trend was independent of the temperature.

Next we measured ^{55}Fe spectra for each pixel at 20°C and energy resolutions for 5.9 keV emission line at various bias voltages. The signals from the APD are connected to a charge sensitive amplifier (581K, Clearpulse) and a shaping amplifier of $\tau = 0.5\ \mu$s (Model 590, ORTEC), then recorded by a peak-holding ADC (V006, HOSHIN). An example of ^{55}Fe spectrum is shown in

2012 JINST 7 C03038

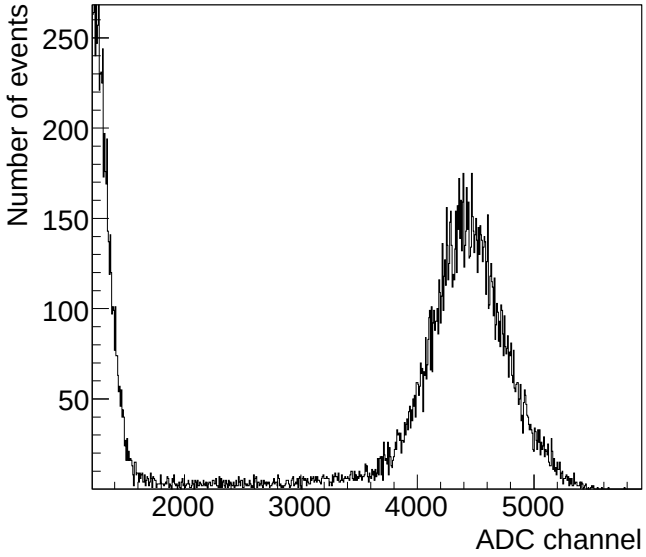

Figure 3. A ^{55}Fe spectrum obtained by pixel ID 5. The measurement is performed at 20°C and bias voltage is 200 V.

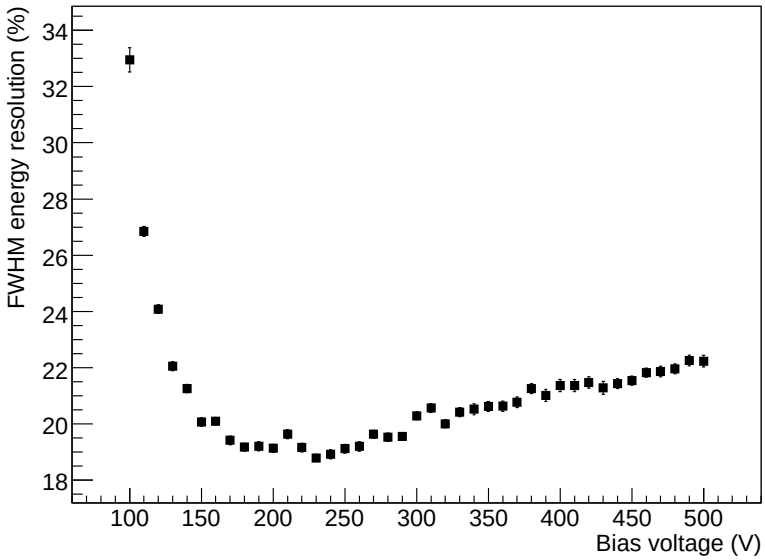

Figure 4. Typical trend of the energy resolution for ^{55}Fe with respect to the bias voltage for the channel ID 5 at 20°C.

figure 3 and we found a typical energy threshold is ∼2 keV at 20°C. We evaluated energy resolution of the 5.9 keV line by fitting with a Gaussian. Figure 4 presents the FWHM energy resolution of the same pixel as figure 3. These values are a little worse than as reported by [10] of 15.7%, because of larger capacitance and dark current due to the larger geometrical size of the APD pixel.

We also compared energy resolutions and relative gain among each pixels using the 5.9 keV line. The measurement was performed at 0°C temperature, assuming a typical thermal circum-

2012 JINST 7 C03038

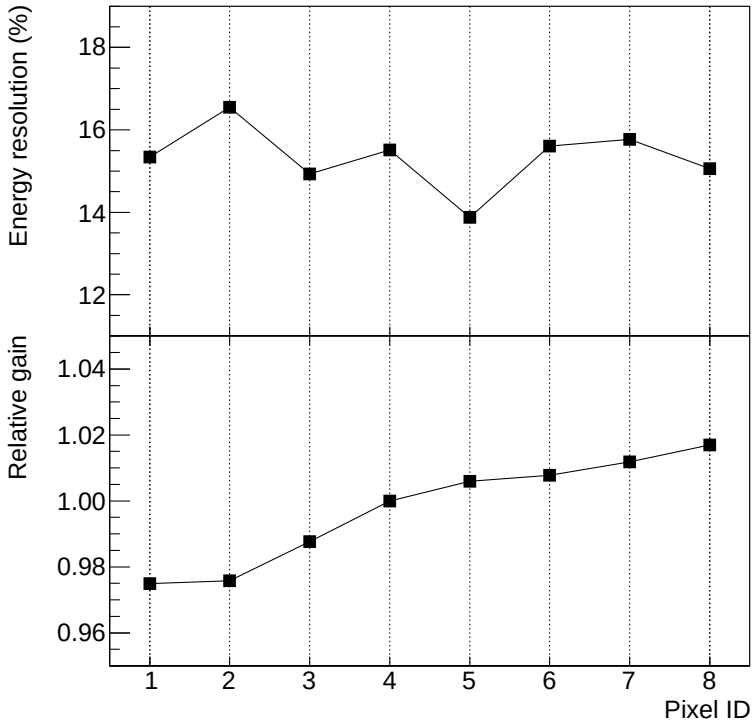

Figure 5. FWHM Energy resolutions (top) and relative gains (bottom) for each pixel, evaluated by 5.9 keV line of ^{55}Fe at 0°C. The relative gains are normalized by the pixel 4.

stance in a space mission. We plotted the energy resolutions in figure 5 (top), which are distributed between from 13.9 to 16.5%. The relative gain is calculated from a mean of the fitted Gaussian divided by that of pixel ID 4. The result is presented in figure 5 (bottom) and we found the gain uniformity is guaranteed within ±2%. We found excellent uniformity both of the gains and the energy resolutions which will provide convenient handling of these arrays as a position sensitive detector.

2.2 16 channel array

We have also developed a 16-channel APD array 7004 having narrower pixel width of 1.1 mm as shown in figure 6. Since the area of the APD segment is smaller than that of the 8-channel array, we could expect not only the better positional resolution but also the better energy resolution due to less capacitive noise which is dominant at low temperatures. Here we present characteristic studies of the 16-ch array at 20°C. Dark current variation along with the bias voltage is shown figure 7, where one pixel appears breakdown at lower voltage than others. As well as the 8-ch array, using the 5.9 keV line relative gain and energy resolutions are plotted in figure 8. We confirmed the both uniformity and better energy resolution, where the former is comparable to the 8-ch array and the latter is better as expected. Note that figure 5 is derived from the measurements at 0°C, and the energy resolutions at 20°C are typically ∼22%.

2012 JINST 7 C03038

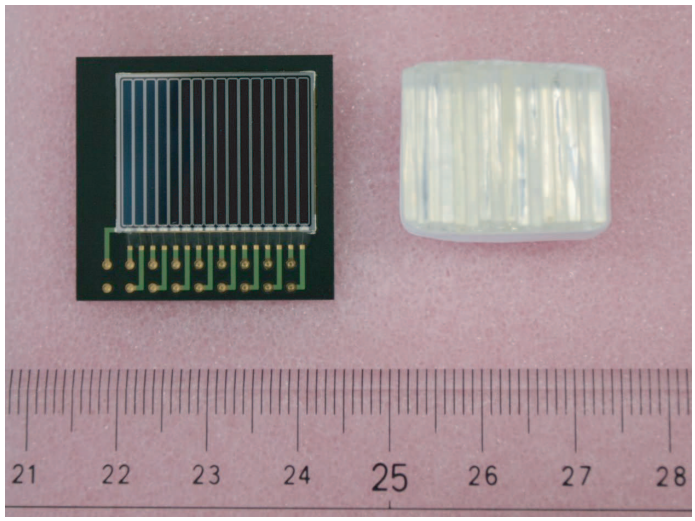

Figure 6. A picture of the 16-channel APD array with a corresponding pixelized CsI(Tl) array.

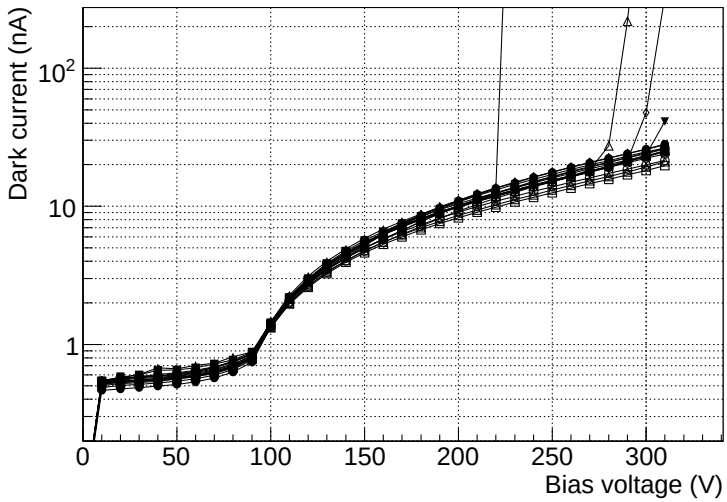

Figure 7. Dark current versus bias voltage for each channel of the 16 channel array.

3 Coupling with CsI scintillators

In order to demonstrate the wide-band energy coverage, we followed [10] using these APD arrays. First we fabricated CsI(Tl) scintillators to fit to the APD pixel sizes whose dimension is $2.2 \times 10.0 \times 16.0$ mm^3 for each as shown in figure 1. Then we individually wrapped a segment of CsI(Tl) with commercially available Enhanced Specular Reflector (ESR, 3M) for the purpose of the optical isolation from neighboring crystals. These scintillators are bundled by Teflon tapes and optically coupled to the APD arrays with silicone grease. Signals from the CSA are fed in parallel into fast ($\tau = 50$ ns) and slow ($\tau = 2\mu$s) shaping amplifier. The data acquisition system (DAQ) is triggered by the fast signal of a single channel and records both the fast and slow signals for all channels.

2012 JINST 7 C03038

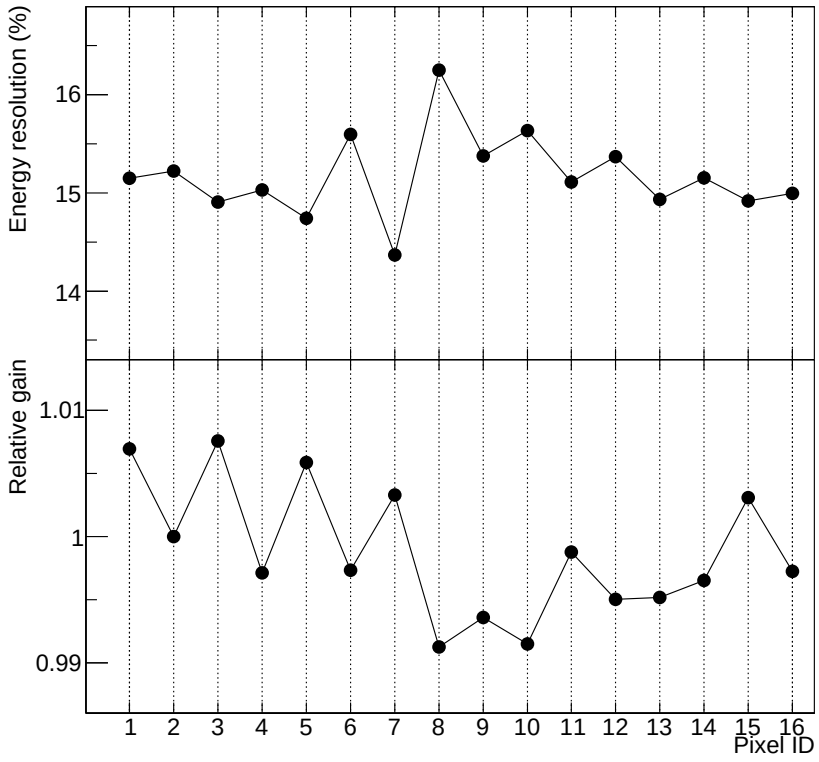

Figure 8. FWHM energy resolutions (Top) and relative gains of the 16 channel array measured by 5.9 keV line at 20°C. The relative gains are normalized by ID 2.

Next, the stacked detector was exposed to a ^{137}Cs gamma-ray source at 0°C. Figure 9 shows a pulse-height correlation between responses of the fast and slow shaping amplifiers obtained by pixel ID 5, triggered by the same channel. The steeper elongated component corresponds to gamma-ray events absorbed by the CsI(Tl) crystal, while the flatter distribution are X-rays directly detected by the APD. We demonstrated that the two components are clearly separated. Then we select events between solid lines in figure 9 as CsI-hit and APD-hit events. Hereafter we only treat these reduced events and extract spectra by projecting to the cut lines. In order to avoid confusions we exclude events which satisfy both the CsI- and APD-hit selection criteria at lowest energies.

A possible problem is a cross-talk effect mainly due to scintillation light leakages from neighboring pixels, where we estimate as follows. When we obtained the data shown in figure 9, the DAQ was configured to be triggered by the signal only from the pixel ID 5 and simultaneously recorded spectra of all the 8 channels. In this case, light leakages from ID 4 and 6 could also trigger the system. In order to identify events with gamma rays absorbed in the CsI of ID 4 and 6, we first extracted CsI-hit energy spectra of these pixels where photoelectric absorption peaks were clearly seen for each spectrum Then we selected such events and extracted CsI-hit spectrum of ID 5 that corresponds to events contaminated from the neighbors. Figure 10 shows CsI-hit spectrum of ID 5, together with the contamination from the photoelectric-absorption events in the channel 4 and 6 presented by dashed and hatched-dashed histograms, respectively. The contamination events

2012 JINST 7 C03038

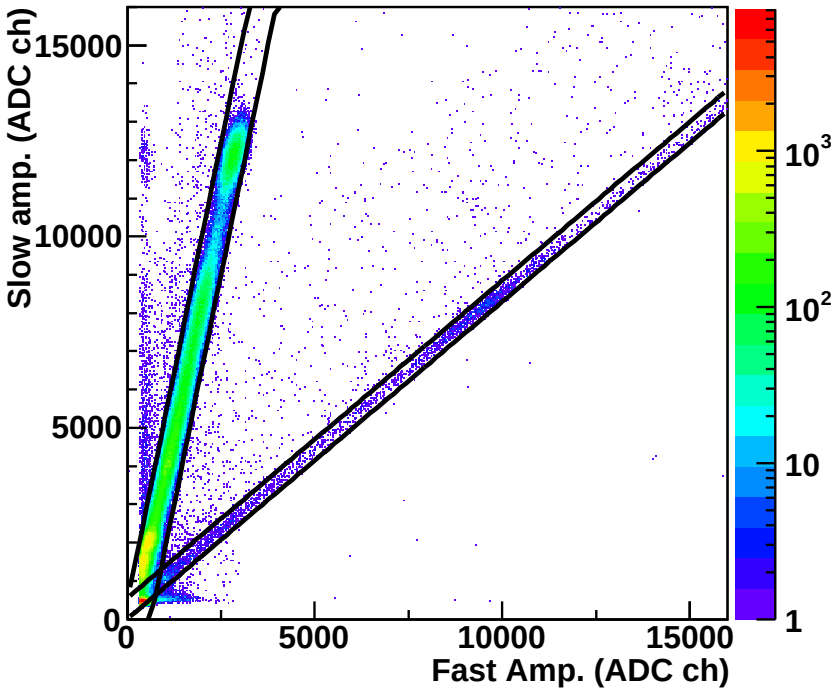

Figure 9. Two dimensional spectrum of ^{137}Cs at 0°C. Vertical and horizontal axes correspond to the recorded pulse height from the slow and fast amplifier, respectively. *z*-axis is in a logarithmic scale. Solid lines represent the event selection criteria described in the text. The steeper and flatter branches correspond to CsI- and APD-hit events, respectively.

should be equivalent around 70 keV that indicates the scintillation light leakage should be $\sim 10\%$ and does not affect an energy resolution of the 662 keV peak. We also checked that contributions from further pixels are negligible. Therefore we confirmed that we can sufficiently determine the incident gamma-ray position by searching a channel with the maximum pulse height.

We excluded the contaminated events and finally obtained the source spectrum over ~ 3 orders of magnitude as shown in figure 11 using both the APD- and CsI-hit events. The energy resolution at 662 keV is 8.4% for this channel and less than 9 keV for the other channels. For 32/36 keV peak 8.0% is achieved by the direct APD measurement.

We should extend the covering length along with the corresponding axis by arranging several number of the APD arrays in order to have a sufficient effective area in future missions. For processing the larger number of readout channels, using a number of the 16-channel arrays for instance, we have developed a dedicated high performance 32-ch analog VLSI specialized for the APD array readout (VATA462, Gamma Medica Inc.). VATA462 provides a CSA, a trigger generator, a shaping amplifier, and an internal ADC for each channel. Since the reach-through type APD has a large capacitance as described above, the VLSI should have low capacitive gradient in the noise profile. VATA462 has as low equivalent noise charge of 200 $e^- + 8$ e^-/pF as expected. Yatsu et al.(2011) demonstrated the performance of VATA462 as a CsI(Tl) signal readout with a reverse type APD [11]. The achieved energy resolution for 662 keV is superior to the commercially available very low noise CSAs such as 581K (ClearPulse) also used this work. VATA462 has proved

2012 JINST 7 C03038

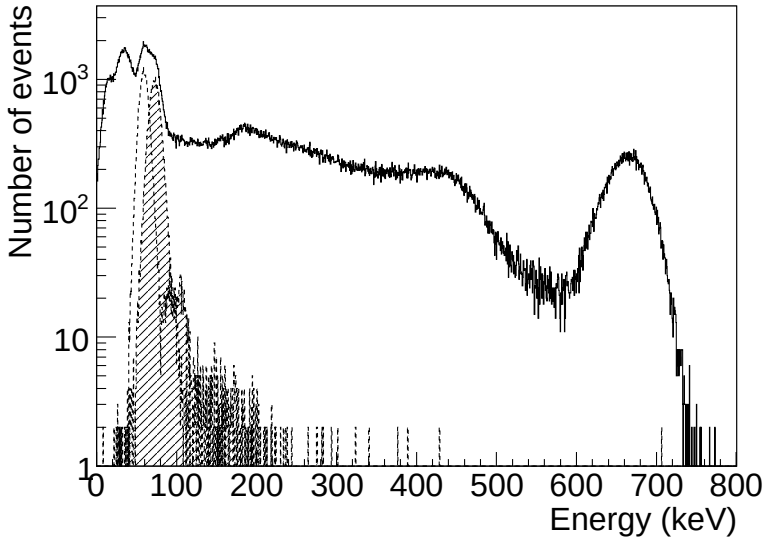

Figure 10. ^{137}Cs spectrum detected by CsI(Tl) and light leakage from neighboring pixel, obtained by the pixel ID 5. Contributions of the photo-electric absorption at pixel ID 4 (dashed) and 6 (dotted) are also presented (see text).

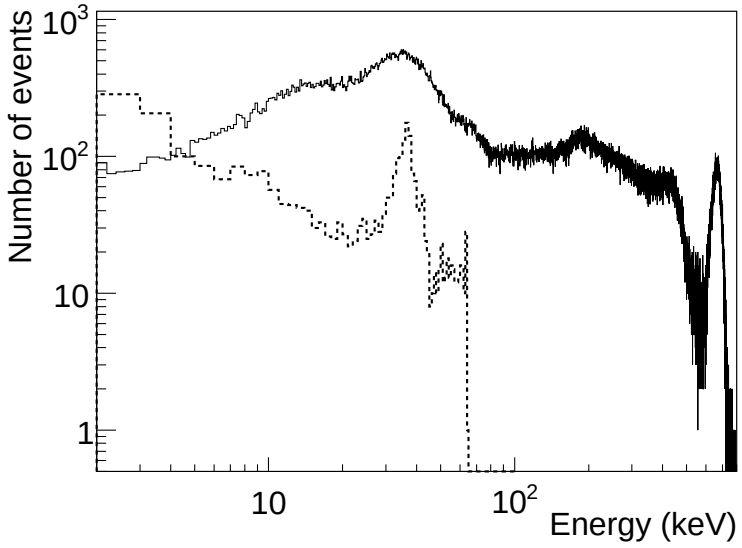

Figure 11. ^{137}Cs spectra obtained by the channel 5. Solid and dashed histograms correspond to CsI and APD-hit events, respectively.

to be a promising readout device, particularly suitable for when we extend the APD array for larger coverage. By nature VLSI is a compact device with low power consumption thus VATA462 is quite favorable for space missions including pico-satellite mission with strict constrains on weight, space and powers.

2012 JINST 7 C03038

4 Conclusion and prospects

We developed the reach-through type APD array manufactured by Hamamatsu to be applied for a position-sensitive wideband X-ray/Gamma-ray spectrometers, mainly for the purpose of observations of astrophysical transient phenomena. We studied the basic characteristics of the APD array of 2.2 mm$\times$16.0 mm$\times$8 and 1.1 mm$\times$16.0 mm$\times$16 pixels, and confirmed using the 5.9 keV emission line that the APD array has a uniform gain ($\pm$2%) and energy resolution over the pixels. Together with the CsI(Tl) array we demonstrated wideband coverage from a few keV to $\sim$1 MeV. The scintillation light contamination from adjacent pixels is at $\sim$ 10% level, which does not affect determination of the interaction point. These results demonstrate the excellent performance of the APD array as a 1-dimensional position sensitive detector. The positional resolution should be identical to the pixel width of 2.2 mm for the 8-channel array, which could be improved by the 16-channel arrays. When we integrate the APD arrays, the readout electronics with VATA462 and coded masks to be designed, the detector has a great potential to be applied to various space missions.

Acknowledgments

We thank the anonymous referees for their careful reading and comments that significantly improved the manuscript. This work is supported by Grants-in-Aid for Scientific Research in Priority Areas “Gamma-Ray Bursts” from the Ministry of Education, Culture, Sports, Science and Technology of Japan No. 19047001.

References

[1] T. Ikagawa et al., *Performance of large area avalanche photodiode for low-energy X-rays and gamma rays scintillation detection*, *Nucl. Instrum. Meth.* **A 515** (2003) 671.

[2] T. Ikagawa et al., *Study of large area Hamamatsu avalanche photodiodes in a gamma-ray scintillation detector*, *Nucl. Instrum. Meth.* **A 538** (2005) 640.

[3] J. Kataoka et al., *An active gain-control system for avalanche photo-diodes under moderate temperature variations*, *Nucl. Instrum. Meth.* **A 564** (2006) 300.

[4] T. Takahashi et al., *The ASTRO-H mission*, *Proc. SPIE* **7732** (2010) 27.

[5] M. Kokubun et al., *Hard X-ray and gamma-ray detector for ASTRO-H based on Si and CdTe imaging sensors*, *Nucl. Insrum. Meth.* **A 623** (2010) 425.

[6] H. Tajima et al., *Soft Gamma-ray Detector for ASTRO-H mission*, *Proc. SPIE* **7732** (2010) 34.

[7] J. Kataoka et al., *In-orbit performance of avalanche photodiodes as radiation detector onboard the Pico-satellite Cute-1.7+APD II*, *J. Geophys. Res.* **115** (2009) A05204.

[8] Y. Yatsu et al., *Study of avalanche photodiodes for soft X-ray detection below 20 keV*, *Nucl. Insrum. Meth.* **A 564** (2006) 134.

[9] Y. Shirasai et al., *Design and Performance of the Wide-Field X-Ray Monitor on Board the High-Energy Transient Explorer 2*, *Publ. Astron. Soc. Japan* **55** (2003) 1023.

[10] S. Tanaka et al., *Development of wideband X-ray and gamma-ray spectrometer using transmission-type, large area APD*, *Nucl. Instrum. Meth.* **A 582** (2007) 562.

[11] Y. Yatsu et al., *Development micro-satellite TSUBAME for polarimetry of gamma-ray bursts*, *Proc. SPIE* **8145** (2011) 8.

2012 JINST 7 C03038